Photoionization of the scandium atom. II. Classifications

F. Robicheaux* and Chris H. Greene
Department of Physics and Joint Institute for Laboratory Astrophysics, University of Colorado, Boulder, Colorado 80309-0440
(Received 1 April 1993)

In this paper we use the calculated photoabsorption cross section and scattering parameters to classify most of the autoionizing lines reported by Garton *et al.* [Proc. R. Soc. London Ser. A **333**, 1 (1973)]. This study proves the capability of eigenchannel R-matrix calculations to provide spectroscopically useful information on the complicated spectra of transition-metal atoms. We present cross sections for the six optically allowed combinations $4s^2 3d\,^2D_{3/2,5/2} \rightarrow 1^o/2, 3^o/2, 5^o/2, 7^o/2$ from near the $(4s3d)^3D$ thresholds to the $(3d^2)^3F$ thresholds.

PACS number(s): 32.80.Fb, 31.20.Di, 32.80.Dz

I. INTRODUCTION

The preceding paper describes general aspects of Sc photoionization dynamics in the low-energy autoionizing region [1]; the transition-metal atoms have rarely been studied in this region of their spectrum. The theoretical description of the spectra is complicated by the large number of closely spaced thresholds; the Rydberg series interact with each other producing a complicated spectrum. The calculated scattering parameters need to be very accurate to place the perturbers in the correct positions; the theoretical spectrum can appear very different even if the perturber has only a small error in its quantum defect (because the error in the position of the perturber is $[\Delta\omega \text{ (a.u.)}] = \Delta\mu/\nu^3$, where the effective quantum number ν is comparatively small in the perturbing channel). The lessons learned in the theoretical treatment of Sc may apply to the other transition metals since the valence shell for all of these elements is composed of s and d orbitals.

The focus of this paper is on the detailed classification of the autoionizing lines reported by Garton *et al.* [2] (GRTE). We present theoretical spectra for photoionization from the $^2D_{3/2,5/2}$ ground electronic states along with the positions of some experimental lines marked by vertical lines; this comparison can indicate the level of agreement between theory and experiment. The results reported here are complementary to those reported earlier [1]; a better understanding of Sc can be obtained by studying both the fine-scale details and the large-scale dynamics. The following paper predicts the photoionization of an even-parity Sc excited state and compares to experimental cross sections from threshold to the ^3F thresholds; comparison of the cross sections for photoabsorption from two different initial states adds insight into the dynamics.

The results presented in this paper show that the eigenchannel R-matrix technique achieves the accuracy needed for the theoretical description of the complex spectra of transition-metal elements. This method has already produced many spectroscopically useful results for complex spectra of the alkaline earths and for several atoms with open p subshells. However, the density (in energy) of thresholds for the transition-metal atoms near the ionization threshold is an order of magnitude larger than for any of the other elements that have been attempted; the spectra are extremely complicated by perturbers, even near the lowest thresholds. The results presented in this paper represent a breakthrough in the description of autoionizing spectra; it seems probable that an accurate treatment of the other (more complicated) transition metals can be achieved in the near future, as well as a fuller theoretical understanding.

The same theoretical and numerical techniques have been used as in our previous articles [1,3,4]. The techniques are "nearly" *ab initio*; effects of the 18 core electrons are described using a screened Coulomb potential [5] with a dipole polarizability that gives the correct energies of the one-electron-like ion Sc III. We solve for the three-electron valence wave function with the streamlined version [6] of the eigenchannel R-matrix technology in an R-matrix volume $r_1, r_2, r_3 < 21$ a.u. We match these solutions onto Coulomb functions at the surface of this volume to obtain the scattering parameters [7]. Spin-orbit effects are incorporated through the LS-jj frame transformation [8] using empirical fine-structure splittings of the Sc^+ thresholds. In the calculation of the short-range scattering parameters we use the theoretical thresholds; however, in the calculation of the cross section which uses these parameters we input the experimental thresholds. The photoionization cross sections are calculated in both length and velocity gauges as a check on the accuracy; poor agreement between the two cross sections would indicate uneven convergence.

II. Sc TARGET STATES AND CHANNELS

We are interested in the photoionization from the electronic ground state, $(4s^2)^1S3d\,^2D_{3/2,5/2}$. This state has a modest amount of configuration interaction as described in Ref. [1]. In all that follows these states will be abbreviated to $^2D_{3/2}$ and $^2D_{5/2}$, or simply 3/2 and 5/2. For comparison, the final states will be designated by $1^o/2$,

 ©1993 The American Physical Society

TABLE I. Experimental threshold wavelengths from the $J_g = 3/2$ and $J_g = 5/2$ states from Ref. [9].

Configuration	$\lambda_{3/2}$ (nm)	$\lambda_{5/2}$ (nm)
$(4s3d)^3D_1$	188.957	189.560
$(4s3d)^3D_2$	188.715	189.316
$(4s3d)^3D_3$	188.324	188.923
$(4s3d)^1D_2$	180.299	180.848
$(3d^2)^3F_2$	173.235	173.741
$(3d^2)^3F_3$	172.993	173.498
$(3d^2)^3F_4$	172.682	173.185
$(3d^2)^1D_2$	156.576	156.990
$(4s^2)^1S_0$	154.658	155.062
$(3d^2)^3P_0$	153.855	154.254
$(3d^2)^3P_1$	153.790	154.189
$(3d^2)^3P_2$	153.665	154.063
$(3d^2)^1G_4$	148.846	149.220

$3^o/2$, $5^o/2$, and $7^o/2$.

In Table I we give the wavelengths of the various thresholds [9] that are important in the energy range discussed in this paper. Where there is no chance for confusion, we abbreviate the ionic target state by $^{2S+1}L_{J_c}$. The final states were constructed by adding p- and f-wave electrons onto these states; similarly s-, d-, and g-wave electrons were added onto the odd-parity target states at higher energies [1]. We also included configuration interaction among the ionic target states, and among the initial and final three-electron atomic states.

III. THEORETICAL CROSS SECTIONS

In Figs. 1–4 we present the theoretical cross sections for the six optically allowed transitions $3/2,\ 5/2 \rightarrow 1^o/2,\ 3^o/2,\ 5^o/2,\ 7^o/2$. At the top of the figures are lines that mark the experimental positions of the autoionizing lines observed by Garton *et al.* The different series are indicated with different types of lines.

There are several places on Figs. 1–4 where it is difficult to identify the correspondence between the calculated and experimental autoionizing resonances; however, there are several states where it is easy to identify the correspondence and it was from these states that we originally estimated the errors in the scattering parameters. For example, it is relatively easy to identify the correspondence between the calculated and experimental lines of series 6 and 7 of Garton *et al.* as well as for the first ~ 10 lines of Fig. 3.

We do not give classifications of the calculated lines on Figs. 1–4 to avoid overcrowding the figures with symbols. The preceding paper [1] classifies the major spectral features. We plot both the length (solid line) and velocity (dashed line) gauge cross sections; the comparison between the two is one indicator of the level of convergence because if the ground or final states were not converged these two cross sections would not normally agree.

For some of the experimental lines, the corresponding theoretical line is fairly obvious. For others, the correspondence was less obvious and heuristic principles discussed below allowed a classification for most of the remaining lines. Though these principles serve as a reasonable guide, they should not be considered a replacement for a proper comparison between a continuous experimental cross section and the theoretical cross section. Experimental information on the widths and shapes of the autoionizing lines is an invaluable aid for the theoretical classification of the experimental lines.

IV. CLASSIFICATIONS OF AUTOIONIZING LINES

Garton *et al.* [2] provided several tables of autoionization lines. For most of the lines they were able to determine the total angular momentum of the initial state, J_g, by finding pairs of lines with the ground state splitting. Almost all of their assignments of J_g were correct; in a complex spectrum, there will "accidentally" be pairs of lines with an energy splitting equal to that of the ground state. They were able to group most of their lines into Rydberg series attached to different thresholds. They

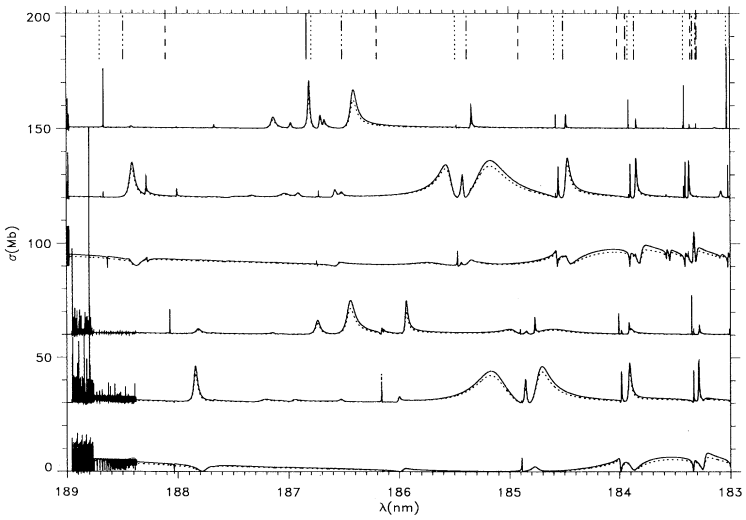

FIG. 1. The theoretical photoionization cross section for Sc in the length (solid line) and velocity (dashed line) gauges. The experimental energies of the lines of series 3 are marked with long-dashed vertical lines, of series 4 with dash-dot-dot-dot vertical lines, of series 5 with dash-dot vertical lines, of series 6 with short-dashed vertical lines, of series 7 with dotted vertical lines, and of series 8 with solid vertical lines. We have added 30 Mb to the $3/2 \rightarrow 3^o/2$ cross section, 60 Mb to the $3/2 \rightarrow 5^o/2$ cross section, 90 Mb to the $5/2 \rightarrow 3^o/2$ cross section, 120 Mb to the $5/2 \rightarrow 5^o/2$ cross section, and 150 Mb to the $5/2 \rightarrow 7^o/2$ cross section.

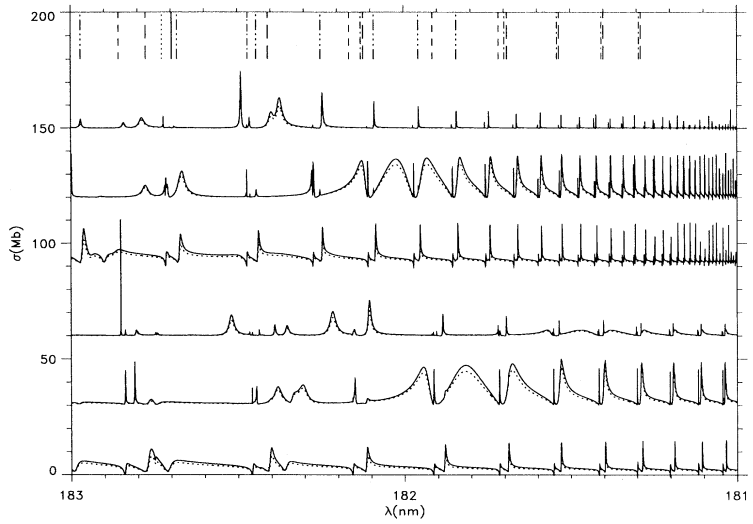

FIG. 2. Same as Fig. 1 except different wavelength range.

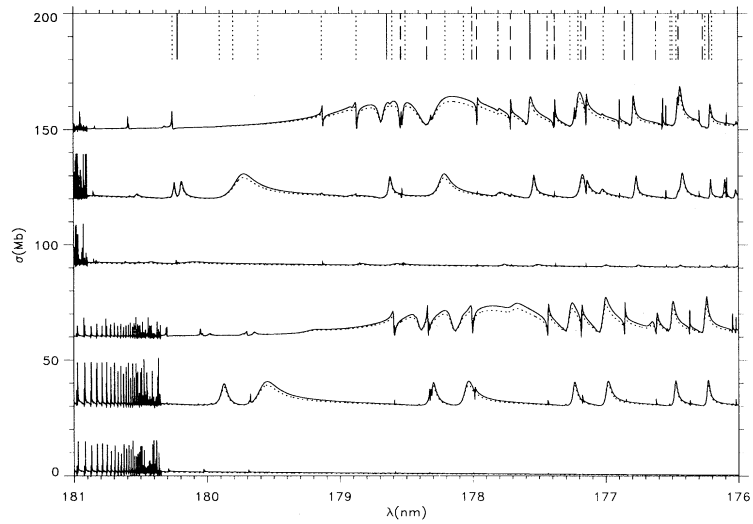

FIG. 3. The theoretical photoionization cross section for Sc in the length (solid line) and velocity (dashed line) gauges. The experimental energies of the lines of series 8 are marked with solid vertical lines, of series 2 by short-dashed vertical lines, of $3/2 \rightarrow J_f^o$ of Table 6 by dash-dot-dot-dot vertical lines, of $5/2 \rightarrow J_f^o$ of Table 6 by long-dashed vertical lines, and of Table 7 of GRTE by dotted vertical lines. We have added 30 Mb to the $3/2 \rightarrow 3^o/2$ cross section, 60 Mb to the $3/2 \rightarrow 5^o/2$ cross section, 90 Mb to the $5/2 \rightarrow 3^o/2$ cross section, 120 Mb to the $5/2 \rightarrow 5^o/2$ cross section, and 150 Mb to the $5/2 \rightarrow 7^o/2$ cross section.

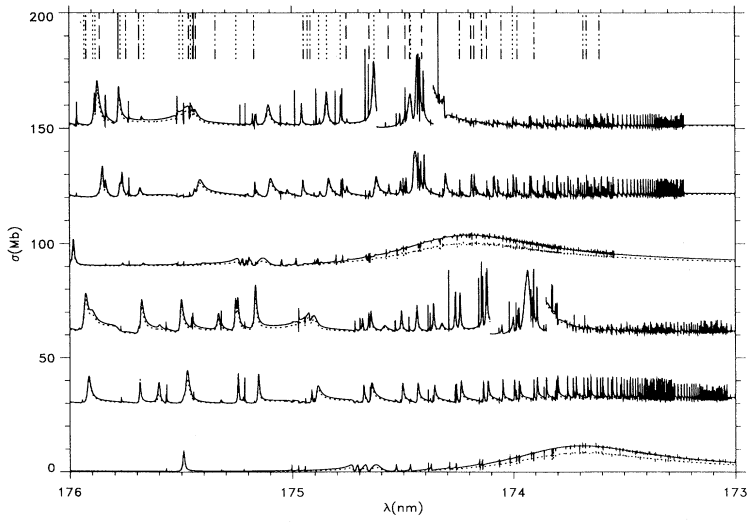

FIG. 4. Same as Fig. 3 except different wavelength range. A short section of the third curve and part of the sixth curve have been divided by 10 for clarity.

TABLE II. Theoretical classifications that differ from or complete the classifications for the low-lying autoionization lines of Garton *et al.* We assume the theoretical classification of Rydberg series do not change above those given in this table. The experimental wavelength and energy above ground state are listed along with the number of the appropriate table of Garton *et al.* We are not as confident of the classifications of the lines with "?"; the reason for the uncertainties is discussed in the proper section of the text.

Table	λ (nm)	$E(\mathrm{cm}^{-1})$[a]	Classification
1	174.467	57485.7	$5/2 \rightarrow 7^o/2\ ^3F_4 18p$
1	174.412	57503.8	$5/2 \rightarrow 7^o/2\ ^1S4f\ ^2F^o$
2	183.940	54365.6	$3/2 \rightarrow 3^o/2\ ^1D12p\ ^2D^o$
2	183.297	54556.2	$3/2 \rightarrow 3^o/2\ ^1D13p\ ^2D^o$
2	182.776	54711.8	$3/2 \rightarrow 1^o/2\ ^1D14p\ ^2P^o$
2	182.408	54822.2	$3/2 \rightarrow 1^o/2\ ^1D15p\ ^2P^o$
2	182.122	54908.2	$3/2 \rightarrow 1^o/2\ ^1D16p\ ^2P^o$
2	181.691	55038.5	$3/2 \rightarrow 1^o/2\ ^1D18p\ ^2P^o$
2	181.534	55085.9	$3/2 \rightarrow 1^o/2\ ^1D19p\ ^2P^o$
2	181.400	55126.6	$3/2 \rightarrow 1^o/2\ ^1D20p\ ^2P^o$
2	181.288	55160.8	$3/2 \rightarrow 1^o/2\ ^1D21p\ ^2P^o$
2	188.485	53222.9	$5/2 \rightarrow 5^o/2\ ^1D9p\ ^2D^o$
2	186.51	53784	$5/2 \rightarrow 7^o/2\ ^1D10p\ ^2F^o$
2	185.379	54111.8	$5/2 \rightarrow 7^o/2\ ^1D11p\ ^2F^o$
2	184.504	54367.7	$5/2 \rightarrow 5^o/2\ ^1D12p\ ^2D^o$
2	183.862	54556.9	$5/2 \rightarrow 5^o/2\ ^1D13p\ ^2D^o$
3	183.306	54553.4	? $3/2 \rightarrow 1^o/2\ ^1D13p\ ^2P^o$
3	182.129	54906.2	? $3/2 \rightarrow 3^o/2\ ^1D16p\ ^2D^o$
3	181.698	55036.4	$3/2 \rightarrow 3^o/2\ ^1D18p\ ^2D^o$
3	181.540	55084.2	$3/2 \rightarrow 3^o/2\ ^1D19p\ ^2D^o$
3	181.406	55125.0	$3/2 \rightarrow 3^o/2\ ^1D20p\ ^2D^o$
3	181.293	55159.2	$3/2 \rightarrow 3^o/2\ ^1D21p\ ^2D^o$
4	188.101	53162.7	$3/2 \rightarrow 5^o/2\ ^1D7f\ ^2F^o$
4	186.195	53707.1	$3/2 \rightarrow 3^o/2\ ^1D8f\ ^2D^o$
4	184.912	54079.5	$3/2 \rightarrow 5^o/2\ ^1D9f\ ^2F^o$
4	184.014	54343.6	$3/2 \rightarrow 5^o/2\ ^1D10f\ ^2F^o$
4	183.354	54539.3	$3/2 \rightarrow 5^o/2\ ^1D11f\ ^2F^o$
4	182.857	54687.5	$3/2 \rightarrow 5^o/2\ ^1D12f\ ^2F^o$
4	182.469	54803.6	$3/2 \rightarrow 5^o/2\ ^1D13f\ ^2F^o$
4	182.164	54895.3	$3/2 \rightarrow 5^o/2\ ^1D14f\ ^2F^o$
4	181.914	54970.8	$3/2 \rightarrow 3^o/2\ ^1D15f\ ^2D^o$
4	181.716	55030.7	$3/2 \rightarrow 3^o/2\ ^1D16f\ ^2D^o$
4	188.698	53162.8	$5/2 \rightarrow 7^o/2\ ^1D7f\ ^2F^o$
4	186.785	53705.7	$5/2 \rightarrow 5^o/2\ ^1D8f\ ^2D^o$
4	185.486	54080.5	$5/2 \rightarrow 7^o/2\ ^1D9f\ ^2F^o$
4	184.585	54343.6	$5/2 \rightarrow 7^o/2\ ^1D10f\ ^2F^o$
4	183.921	54539.3	$5/2 \rightarrow 7^o/2\ ^1D11f\ ^2F^o$
4	183.420	54687.8	$5/2 \rightarrow 7^o/2\ ^1D12f\ ^2F^o$
4	183.034	54802.9	$5/2 \rightarrow 7^o/2\ ^1D13f\ ^2F^o$
4	182.727	54894.6	$5/2 \rightarrow 7^o/2\ ^1D14f\ ^2F^o$
5	186.830	53692.6	$5/2 \rightarrow 7^o/2\ ^3F7p\ ^2F^o$
5	182.697	54903.5	$5/2 \rightarrow 5^o/2\ ^3F_3 8p$
5	180.216	55657.2	$5/2 \rightarrow 5^o/2\ ^3F_3 9p$
5	178.639	56147.0	$5/2 \rightarrow 5^o/2\ ^3F_3 10p$
5	177.561	56486.9	$5/2 \rightarrow 5^o/2$ and $7^o/2\ ^3F_3 11p$
5	176.788	56733.1	$5/2 \rightarrow 5^o/2$ and $7^o/2\ ^3F_3 12p$
5	176.217	56916.3	$5/2 \rightarrow 5^o/2(?)$ and $7^o/2\ ^3F_3 13p$
5	175.781	57057.2	$5/2 \rightarrow 5^o/2$ and $7^o/2\ ^3F_3 14p$
6	177.999	56180.0	$3/2 \rightarrow 5^o/2\ ^3F_4 8f$
6	177.803	56410.0	$5/2 \rightarrow 5^o/2$ and $7^o/2\ ^3F_2 11p$
6	177.431	56359.7	$3/2 \rightarrow 5^o/2\ ^3F_2 9f$
6	177.178	56440.3	$3/2 \rightarrow 5^o/2\ ^3F_3 9f$
6	176.850	56544.9	$3/2 \rightarrow 5^o/2\ ^3F_4 9f$
6	176.615	56620.3	$3/2 \rightarrow 5^o/2\ ^3F_2 10f$
6	175.925	56842.4	$3/2 \rightarrow 3^o/2$ and $5^o/2\ ^3F_2 13p$
6	175.344	57030.6	$3/2 \rightarrow 5^o/2\ ^3F_4 13p$
6	175.170	57087.2	$3/2 \rightarrow 3^o/2$ and $5^o/2\ ^3F_2 15p$
6	174.240	57391.8	$3/2 \rightarrow 3^o/2$ and $5^o/2\ ^3F_2 20p$
6	174.139	57425.3	$3/2 \rightarrow 3^o/2$ and $5^o/2\ ^3F_2 21p$
6	174.051	57454.2	$3/2 \rightarrow 3^o/2$ and $5^o/2\ ^3F_2 22p$
6	173.978	57478.3	$3/2 \rightarrow 3^o/2$ and $5^o/2\ ^3F_2 23p$ and $^3F_4 16f$
6	173.681	57576.8	$3/2 \rightarrow 3^o/2\ ^3F_2 29p$
6	173.666	57581.7	$3/2 \rightarrow 3^o/2\ ^3F_3 24p$
6	173.608	57600.9	$3/2 \rightarrow 3^o/2\ ^3F_3 25p$
6	178.534	56179.9	$5/2 \rightarrow 7^o/2\ ^3F_4 8f$
6	178.338	56073.2	$3/2 \rightarrow 5^o/2\ ^3F_3 8f$
6	177.962	56360.0	$5/2 \rightarrow 7^o/2\ ^3F_2 9f$
6	177.708	56440.2	$5/2 \rightarrow 7^o/2\ ^3F_3 9f$
6	177.378	56544.9	$5/2 \rightarrow 7^o/2\ ^3F_4 9f$
6	177.141	56620.4	$5/2 \rightarrow 5^o/2$ and $7^o/2\ ^3F_4 11p$
6	176.446	56842.5	$5/2 \rightarrow 5^o/2$ and $7^o/2\ ^3F_4 12p$
6	175.864	57030.1	$5/2 \rightarrow 5^o/2\ ^3F_4 13p$
6	175.688	57087.1	$5/2 \rightarrow 5^o/2\ ^3F_2 15p$
6	174.754	57391.5	$5/2 \rightarrow 5^o/2\ ^3F_2 20p$
6	174.651	57257.0	$3/2 \rightarrow 3^o/2$ and $5^o/2\ ^3F_3 16p$
6	174.563	57453.9	$5/2 \rightarrow 5^o/2\ ^3F_2 22p$
6	174.488	57478.7	$5/2 \rightarrow 7^o/2\ ^3F_4 16f$ and $^3F_2 23p$
6	174.189	57577.1	$5/2 \rightarrow 5^o/2\ ^3F_4 20p$
6	174.174	57581.8	$5/2 \rightarrow 5^o/2\ ^3F_3 24p$
6	174.117	57432.4	$3/2 \rightarrow 3^o/2$ and $5^o/2\ ^3F_3 19p$
7	180.254	55645.6	$5/2 \rightarrow 5^o/2$ and $7^o/2\ ^3F_4 7f$
7	179.90	55586	$3/2 \rightarrow 3^o/2\ ^3F9p\ ^4D^o$
7	179.80	55786	$5/2 \rightarrow 5^o/2\ ^3F_4 9p$
7	179.61	55676	$3/2 \rightarrow 3^o/2\ ^3F9p\ ^2D^o$
7	179.13	55994	$5/2 \rightarrow 7^o/2\ ^3F_2 8f$
7	178.869	56075.2	$5/2 \rightarrow 7^o/2\ ^3F_3 8f$
7	178.6[b]	56160	$5/2 \rightarrow 7^o/2\ ^3F_3 10p$ and $^3F_4 8f$
7	178.5	56190	$5/2 \rightarrow 7^o/2\ ^3F_4 10p$
7	178.2	56120	? $3/2 \rightarrow 5^o/2\ ^3F_3 10p$
7	178.06	56161	? $3/2 \rightarrow 3^o/2$ and $5^o/2\ ^3F_3 10p$
7	177.378	56545.1	$5/2 \rightarrow 7^o/2\ ^3F_4 9f$
7	177.26	56414	$3/2 \rightarrow 3^o/2$ and $5^o/2\ ^3F_2 11p$
7	177.20	56602	$5/2 \rightarrow 5^o/2$ and $7^o/2\ ^3F_4 11p$
7	177.00	56497	$3/2 \rightarrow 3^o/2$ and $5^o/2\ ^3F_3 11p$
7	176.506	56655.3	$3/2 \rightarrow 5^o/2\ ^3F_2 12p$
7	176.493	56659.5	$3/2 \rightarrow 3^o/2\ ^3F_2 12p$
7	176.463	56837.4	$5/2 \rightarrow 7^o/2\ ^3F_4 12p$
7	175.933	56839.8	$3/2 \rightarrow 3^o/2$ and $5^o/2\ ^3F_2 13p$
7	175.893	57021.1	$5/2 \rightarrow 7^o/2\ ^3F_4 13p$
7	175.883	57024.3	$5/2 \rightarrow 7^o/2\ ^3F_4 13p$
7	175.761	57063.8	$5/2 \rightarrow 5^o/2$ and $7^o/2\ ^3F_3 14p$
7	175.746	57068.3	$5/2 \rightarrow 5^o/2$ and $7^o/2\ ^3F_2 13f$
7	175.689	57087.1	$5/2 \rightarrow 5^o/2\ ^3F_3 13p$
7	175.5060	56978.11	$3/2 \rightarrow 5^o/2\ ^3F_2 14p$
7	175.2500	57229.68	$3/2 \rightarrow 3^o/2$ and $5^o/2\ ^3F_3 14p$
7	174.8774	57351.26	? $5/2 \rightarrow 5^o/2$ and $7^o/2\ ^3F_2 19p$
7	174.842	57362.8	$5/2 \rightarrow 5^o/2$ and $7^o/2\ ^3F_4 16p$

TABLE II. (*Continued*).

Table	λ (nm)	$E(\mathrm{cm}^{-1})$[a]	Classification	Table	λ (nm)	$E(\mathrm{cm}^{-1})$[a]	Classification
7	174.780	57383.1	$5/2 \rightarrow 5^o/2$ and $7^o/2\ ^3F_3 18p$	7	174.463	57487.1	$5/2 \rightarrow 7^o/2\ ^3F_4 18p$
7	174.628	57432.9	$5/2 \rightarrow 5^o/2$ and $7^o/2\ ^3F_4 17p$	7	173.9992	57471.53	$3/2 \rightarrow 5^o/2\ ^3F_3 20p$

[a]Above ground state.
[b]Misprinted as 1686 Å.

classified these series by comparing the quantum defects of the series to those of classified bound states. For one table of lines, they were only able to classify J_g; the final table of lines had no classifications.

In this section we present our classification of the lines measured by Garton *et al.* We were able to classify most of their unclassified lines and complete the classification for their partially classified lines. We are mostly in agreement with the experimental classifications although there are some discrepancies. We present the theoretical classifications that differ from or complete the classifications of Garton *et al.* in Table II.

Our theoretical classification of the experimental lines was performed visually. We plotted the six theoretical cross sections as in Figs. 1–4 but on a much smaller wavelength scale, typically 0.1–0.5 nm. We then drew vertical lines from top to bottom at the experimental energies for the lines that were supposed to lie in that energy range. We then visually paired the experimental and theoretical lines to give the "best agreement." The criteria used to determine the "best agreement" were (1) the difference in the quantum defects of the experimental and theoretical lines should be no greater than 0.05; (2) the difference in quantum defect should not radically change in a Rydberg series (for example, the difference in the quantum defect for a $9p$ state should be roughly equal to the difference for the $10p$ state of the same series); (3) for two theoretical lines "equally close" to an experimental line choose the classification that has the experimentally determined J_g; (4) if two theoretical lines that are "equally close" to an experimental line have greatly different oscillator strengths, choose the more intense line; and (5) match the experimental width and asymmetry of a line to that of the theoretical line.

Once the correspondence between a theoretical and experimental line was successfully established we classified the theoretical line using the short range scattering parameters and multichannel quantum-defect theory. This was accomplished by throwing away all of the open channels in the calculation, thus converting the problem to a search for bound states. Over the width of each resonance we searched for the positions of bound states by finding the zeros of $\det[K_{cc} + \tan(\pi\nu_c)]$ where K_{cc} is the closed-closed part of the reaction matrix and ν_c is the effective quantum number. If more than one bound state happened to fall within the width of the resonance, we chose the bound state that had the largest oscillator strength. (In the ambiguous cases analyzed, there was always one state with much more oscillator strength than the others.) Once the bound state was found we calculated the real-valued vector that satisfied $[K_{cc} + \tan(\pi\nu_c)]\mathbf{V} = \mathbf{0}$. For a given bound state, the probability for finding the Rydberg electron in channel i is proportional to $\nu_i^3 V_i^2 / \cos^2 \pi\nu_i$. We were able to determine the principal quantum number for each state simply by noting that unperturbed p waves had quantum defects near 2 and unperturbed f waves had quantum defects near 0.1.

We were able to classify most of the lines reported by Garton *et al.* [2]. Several lines could not be classified owing to uncertainties in the calculation. As mentioned above, there is a relatively high density of low-n perturbers in this region of the spectra. It was a crucial aspect of the theoretical classification to estimate the acceptable error in the positions of the perturbers and to estimate from the scattering probability matrix how strongly a perturber interacts with various Rydberg series. An example of this is the $(3d^2)^1D4f^2D^o$ state that theoretically fell at 176.108 nm and had non-negligible oscillator strength. An error of 0.01 in the quantum defect for this state would correspond to an error of ~ 0.1 nm. Unfortunately, this line was in the energy range of Rydberg states attached to the $^3F_{J_c}$ thresholds and none of the lines that fell within ~ 0.1 nm of 176.108 nm could be classified. As another example, the perturber $^3F8p^2D^o_{3/2}$ near 181.8 nm interacts much more strongly with the $^1Dnp^2D^o_{3/2}$ Rydberg series than with the $^1Dnf^2D^o_{3/2}$ Rydberg series. Therefore, we find (as expected) that the quantum defects for the np series are much less accurate than those for the nf series.

We classified all of the experimental lines that we could match to one or two theoretical lines irrespective of the theoretical purity of the lines. Several of the lines of Tables 5–7 of Garton *et al.* could not be matched to *one* theoretical line; for these there were usually two theoretical lines (degenerate within the widths of the lines) of nearly equal oscillator strength that corresponded to the same experimental line. For these lines we concluded that the experimental lines were the superposition of two lines. Several of the lines had low purity [1] (especially the $^3F_{J_c}nl$ lines). All of the lines can be classified in either LS or jj coupling, but we always present the classification in the coupling scheme for which the state is purest. For example, the states of Tables 2–4 of Garton *et al.* are presented in LS coupling because they are very pure in this coupling but very heavily mixed in jj coupling.

There are several lines in Tables 1–3 of Garton *et al.* that are listed as obscured. We think that most of these lines were not *obscured* but *perturbed.* Lines can be obscured by other lines of different types of atoms or for the same types of atoms but different symmetries; perturbed lines arise through the interaction of two states of

the same atom and symmetry. Several lines of a Rydberg series can be perturbed by the same state if it is broad enough; over the width of one perturber, the quantum defect of individual lines in the perturbed channel increases by 1. The shapes and widths of the perturbed Rydberg states can also change rapidly with energy. The distinction between perturbed and obscured lines is important for developing an understanding of the atomic dynamics. An obscured line tells you nothing new about the atomic dynamics whereas a perturbed line gives information on the position and width of the perturbing state.

We only present classifications for states up to $n = 21$. The classifications for the higher lying states should not change from those of the $n = 16$–21 levels.

In the tables of Garton *et al.* [2] the lines were frequently paired as having different initial states ($4s^2 3d^2 D_{3/2}$ and $^2D_{5/2}$) with the same final states. However, we have found that the total orbital angular momentum, J_f, of the paired final states were almost always different. As an example, the line at $\lambda = 186.195$ nm was paired with the line at $\lambda = 186.785$ in their Table 4; these lines have total energies above the ground state of 53 707.1 cm^{-1} and 53 705.7 cm^{-1} with their final states classified by us as $(4s3d)^1 D 8f^2 D^o_{3/2}$ and $(4s3d)^1 D 8f^2 D^o_{5/2}$ (these lines were originally classified as $^1D 10p^2 D^o_{3/2,5/2}$?; see Sec. IV D below). The large splitting between these two states does *not* arise arise from the interaction of the spin of the $8f$ electron with its orbital angular momentum but through the interaction of the $8f$ state with a low-n p-wave perturber which is at different energies for $J_f = 3^o/2$ and $J_f = 5^o/2$. The compilation of Sc levels in Ref. [9] averaged the energies of these two states (which is consistent with the original identification [2] of these lines as arising from the same final state) to obtain one line at 53 706.4 cm^{-1}; this compilation probably has small (≤ 1 cm^{-1}) errors due to averaging the energies of lines which were erroneously thought to have the same final state.

A. Table 1 of Garton *et al.*

Garton *et al.* present lines in their Table 1 which they classified as arising from $^2D_{3/2} \rightarrow (4s^2)^1 S n f^2 F^o_{5/2}$ (series 1) and $^2D_{5/2} \rightarrow (4s^2)^1 S n f^2 F^o_{5/2,7/2}$ (series 2). The lowest resonances for these series can be seen on Fig. 4; the line of series 1 is marked by a dash-dot vertical line and the two lines of series 2 are marked by short-dashed vertical lines. We agree with their classifications for series 1. We found [1] that the oscillator strength for $^2D_{5/2} \rightarrow ^1 S n f^2 F^o_{5/2}$ was a factor of 20 smaller than for $^2D_{5/2} \rightarrow ^1 S n f^2 F^o_{7/2}$. This factor of 20 is discussed in Ref. [1] in the section on propensity rules. Since the $5/2 \rightarrow 5^o/2$ lines were so much weaker than and degenerate with the $5/2 \rightarrow 7^o/2$ lines, we feel safe in classifying series 2 as $^2D_{5/2} \rightarrow ^1 S n f^2 F^o_{7/2}$.

We do not agree with the experimental classification of the first two lines of series 2. These were classified as $4s^2 4f^2 F^o_{7/2}$ at 57 317.4 cm^{-1} (174.467 nm) and $4s^2 4f^2 F^o_{5/2}$ at 57 335.5 cm^{-1} (174.412 nm). These are marked by the two short-dashed lines of Fig. 4. The splitting of the $4f$ state of Sc III is $\sim$0.25 cm^{-1}, a factor of 72 smaller than the claimed splitting of the neutral $4f$ state. The upper state (at 57 335.5 cm^{-1}) is 168.4 cm^{-1} below the $^2D_{3/2} \rightarrow 4s^2 4f^2 F^o_{5/2}$ line; we therefore classify this line as the $^2D_{5/2} \rightarrow 4s^2 4f^2 F^o_{7/2}$ transition (the $^2F^o_{5/2}$ state is degenerate with the $^2F^o_{7/2}$ state within the width of the state and the oscillator strength for the $5/2 \rightarrow 5^o/2$ transition is much smaller than that for the $5/2 \rightarrow 7^o/2$ transition). The lower energy line ($\lambda =$ 174.467 nm) is nearly degenerate with the line at 174.463 nm of Table 7 of Garton *et al.*; we have two lines at this wavelength for the $5/2 \rightarrow 7^o/2$ transition with the classification $^3F_4 18p_{1/2,3/2}$. One linear combination of the $p_{1/2}$ and the $p_{3/2}$ states mixes strongly with the $4s^2 4f^2 F^o_{7/2}$ state ($\sim$25% admixture) and therefore is pushed to lower energy and has more oscillator strength; this is the state that we identity with the 57 314.4 cm^{-1} ($\lambda =$ 174.467 nm) line of Table 1 of Garton *et al.* The other linear combination does not mix strongly with the $4s^2 4f^2 F^o_{7/2}$ state (and therefore has less oscillator strength) and we identify this state with the 174.463 nm line of [2] Table 7.

Three lines in [2] Table 1 are listed as obscured; these are $3/2 \rightarrow 5^o/2\ 4s^2 16f$, $5/2 \rightarrow 7^o/2\ 4s^2 16f$, and $5/2 \rightarrow 7^o/2\ 4s^2 20f$. Probably the $4s^2 16f$ states were not obscured. In the calculation the $^1G 8p^2 F^o$ state fell near $4s^2 16f$; a very small change in the quantum defect of the $^1G 8p^2 F^o$ state would make it degenerate with the $4s^2 16f$ state and induce a large perturbation of this series. The $5/2 \rightarrow 7^o/2\ 4s^2 20f$ line is almost equal in wavelength to the $3/2 \rightarrow 5^o/2\ ^1G 8p^2 F^o$ and the $4s^2 16f$ perturbed lines and was probably obscured by them. (The $^1G 7p^2 F^o$ state perturbs the $4s^2 8f$ state.)

The difference between calculated and experimental quantum defects for the $4s^2 nf$ series was less than 0.02 for $n = 4$–15 with the exception of the $3/2 \rightarrow 5^o/2\ 13f$ line which is coincident with the $5/2 \rightarrow 7^o/2\ 15f$ line (probably the experimental error in the quantum defect of the $3/2 \rightarrow 5^o/2\ 13f$ line is 0.01 and the quantum defect should be 0.14).

B. Table 2 of Garton *et al.*

Table 2 of Garton *et al.* presents lines they classified as arising from the $^2D_{3/2} \rightarrow (3d4s)^1 D n p^2 P^o_{3/2}$ (series 3) and $^2D_{5/2} \rightarrow (3d4s)^1 D n p^2 P^o_{3/2}$ (series 4). The resonances of these two series can be found in Figs. 1 and 2; the experimental positions of the resonances of series 3 are marked by long-dashed vertical lines and those of series 4 are marked by dash-dot-dot-dot vertical lines. We agree that the lines are $^1 D n p^2 L_{J_f}$; however, we do not agree with their choice of L and J_f for several of the lines.

The lines that they classify as $^2D_{3/2} \rightarrow ^1\ D n p^2 P^o_{3/2}$ with $n = 12$ and 13, we classify as $^2D_{3/2} \rightarrow ^1\ D n p^2 D^o_{3/2}$. We classify the rest of the lines of series 3 as $^2D_{3/2} \rightarrow ^1 D n p^2 P^o_{1/2}$ with $n = 14$–21; the $^2D_{3/2} \rightarrow\ ^1 D n p^2 P^o_{3/2}$

lines are much weaker [1]. The lines that they classified as $^2D_{5/2} \rightarrow {}^1Dnp^2P^o_{3/2}$ with $n = 9$–13 we classified as $^2D_{5/2} \rightarrow {}^1Dnp^2D^o_{5/2}$ for $n = 9$, 12, and 13 and $^2D_{5/2} \rightarrow {}^1Dnp^2F^o_{7/2}$ for $n = 10$ and 11. The $n = 9$–11 levels of series 3 were not reported and the $n = 8$ levels are below threshold. We agree with their classification for series 4 for $n = 14$–21.

There is some experimental support for changing the classification of series 3 and 4 from $^2D^o$ to $^2P^o$ at $n = 14$; the quantum defects of the $n = 12$ and 13 levels are equal to 2.000 while the quantum defects of the $n = 14$ and 15 levels are equal to 1.914. Figure 1 suggests why the $^2P^o$, $^2D^o$, and $^2F^o$ states were experimentally labeled as part of the same series. In the $^2P^o$ channel the ^1Dnp Rydberg series is perturbed by the ^3P5p state. In the $^2D^o$ channel the ^1Dnp Rydberg series is perturbed by the ^3F8p state. In the $^2F^o$ channel the ^1Dnp Rydberg series is perturbed by the ^3F7p state. Near a perturber the quantum defect changes rapidly with energy. The Rydberg series are found experimentally by grouping together lines that have roughly the same quantum defect. In this heavily perturbed region of the spectrum, the only way to find lines with nearly the same quantum defect was to use lines of different series.

The $n = 17$ line of series 3 is listed as obscured. In the calculated spectrum, the $^3F8p^2D^o$ perturber falls very near the energy of the unperturbed $n = 17$ line. It is a fairly broad and intense line and could have been the state that obscured the $^1D17p^2P^o_{1/2}$ line.

The difference in the experimental and calculated quantum defects for the $^2P^o$ lines was less than 0.03. The differences between experimental and calculated quantum defects for the $^2D^o$ and $^2F^o$ lines were as large as 0.05; however, these were lines that interacted strongly with perturbers and so differences of this size are not surprising.

C. Table 3 of Garton *et al.*

Table 3 of Garton *et al.* presents lines they classified as $^2D_{3/2} \rightarrow (3d4s)^1Dnp^2P^o_{1/2}$ (series 5). Resonances of this series are marked on Figs. 1 and 2; the experimental positions of these resonances are indicated with dash-dot vertical lines. We agree that these lines arise from the $J_g = 3/2$ initial state. In general, we do not agree with their L_f and J_f label.

We remain uncertain what the classification for the $n = 13$ state should be. This wavelength falls very near our $^2D_{3/2} \rightarrow {}^1D13p^2P^o_{1/2}$ line; however, this is a broad structure very close to the $^3P5p^2P^o$ perturber. The $n = 14$ and $n = 15$ lines of this series were not recorded. We have tentatively labeled the $n = 16$ line as $^1D16p^2D^o_{3/2}$; the label is tentative because the difference between the experimental and theoretical quantum defects is ~ 0.07 and the $^2D_{5/2} \rightarrow {}^1D18p^2D^o_{5/2}$ line is much closer in energy but has the wrong J_g. We have chosen the label for the state further away in energy because that label is consistent with what we have labeled the rest of the series; also, the $^3F8p^2D^o$ perturber is strongly interacting with this state which could cause a large error in the quantum defect. We have labeled the $n = 18$–21 states of series 5 $^2D_{3/2} \rightarrow {}^1Dnp^2D^o_{3/2}$.

The $n = 17$ line of series 5 is listed as obscured, but probably it was not. The calculated $^3F8p^2D^o$ state fell very near the energy of the $^1D17p^2D^o$ state and perturbed it strongly. The $^1D17p^2D^o$ state is much broader than the other states of this Rydberg series.

The difference between the experimental and calculated quantum defects for the $n = 13$ state was less than 0.02, for the $n = 16$ state was 0.07, and for the $n = 18$–21 states was 0.04. Probably the interaction between the $^3F8p^2D^o$ state with the $^1Dnp^2D^o$ Rydberg series caused the difference between experimental and theoretical quantum defects to be so large for these states.

The $^1Dnp^2P^o$ and $^2D^o$ states were very close in energy; the difference between the quantum defects of the two series was 0.05–0.09. We chose the classification that preserved the order of the states; the theoretical quantum defect for the $^2P^o$ states was slightly smaller than that for the $^2D^o$ states which is why we labeled most of series 3 $^2P^o$ and most of series 5 $^2D^o$. Finally, the $^3P5p^2P^o$ state did not perturb the $^1Dnp^2P^o$ Rydberg series as strongly as the $^3F8p^2D^o$ perturbed the $^1Dnp^2D^o$ Rydberg series (this may explain why the difference between the experimental and theoretical quantum defects is larger for series 5 than for series 3).

D. Table 4 of Garton *et al.*

Table 4 of Garton *et al.* presents lines that were tentatively classified as arising from $^2D_{3/2} \rightarrow (3d4s)^1Dnp^2D^o_{3/2,5/2}$? (series 6) and $^2D_{5/2} \rightarrow (3d4s)^1Dnp^2D^o_{3/2,5/2}$? (series 7). (The question marks after the classifications indicate the uncertainty of Garton *et al.*) The resonances belonging to these two series are on Figs. 1 and 2; we marked the positions of these resonances with short-dashed lines for series 6 and dotted lines for series 7. We agree with their classification for J_g. However, we do not agree with the np classification nor, in general, with their choice of L_f and J_f.

We found that each of these two series consisted of states from three different symmetries. We also found that all of these resonances had ^1Dnf character. The oscillator strength for the ^1Dnf $^2P^o$, $^2D^o$, and $^2F^o$ symmetries varied considerably over the range of the two series which is why we were forced to assign different states to different symmetries. It is easy to imagine why the three series were identified experimentally as one series, in view of the near identity of the three different quantum defects and the changes in the oscillator strength. In classifying the lines, we considered both the difference in the quantum defect and the theoretical oscillator strength of each line. However, our biggest concern was to minimize the difference between the experimental and theoretical quantum defects; for our assignments, this difference was always less than 0.02 and typically ~ 0.01. We emphasized the quantum defect because these states hardly interact with the other series and they are nf Rydberg states which should have particularly accurate

quantum defects. The oscillator strengths are not determined as accurately because the direct dipole matrix elements to these states are small; a small amount of mixing with a perturber that has a large dipole matrix element can change the oscillator strength by a large factor even when the mixing is too small to affect the quantum defect. There is some experimental justification for this emphasis which is discussed below. The theoretical oscillator strengths are presumably less accurate than the quantum defects.

For series 6, we classified the lines for $n = 9$, 11–16 as $^2D_{3/2} \rightarrow {}^1D(n-2)f^2F^o_{5/2}$. We classified the $n = 10$, 17, and 18 lines as $^2D_{3/2} \rightarrow {}^1D(n-2)f^2D^o_{3/2}$. The $9f$ state was classified with the help of the spectrum from the $(3d^3)^2_3D_{3/2}$ excited state [10] because the $^1D9f^2P^o$ and $^2F^o$ states were nearly degenerate and had roughly equal oscillator strengths. There is some experimental evidence that there is a change of symmetry from $n = 16$ to $n = 17$. Namely, the quantum defects for the $n = 15$ and 16 states are 0.100 and 0.097 while the quantum defects for the $n = 17$ and 18 states are 0.07. For series 7, our classifications are the same as for series 6 with $J_g \rightarrow J_g + 1$ and $J_f \rightarrow J_f + 1$. The $n = 18$ state of series 7 was not reported. The $n = 17$ state of series 7 is at exactly the same wavelength as the $n = 15$ state of series 6. The experimental quantum defect for this state differs by 0.02 from the quantum defect of the corresponding state of series 6; we feel that the error in the experimental quantum defect of the $n = 17$ state of series 7 must be ~ 0.02.

E. Table 5 of Garton *et al.*

Table 5 of Garton *et al.* presents lines they classified as $^2D_{5/2} \rightarrow {}^3F_3np^2L^o$ (series 8). The resonances of this series are on all of the figures; we marked the experimental positions of these resonances with solid vertical lines. We agree with this classification except the $^2L^o$ part which appears not to be meaningful. We find that all of these lines are of the type $^2D_{5/2} \rightarrow {}^3F_3np_{j_o}\ J_f$ with a particular linear combination of j_o and with $J_f = 5/2$ or $7/2$ or both. The np electron can have $j_o = 1/2$ or $3/2$; however, there is no term in the Hamiltonian used for the present calculations that directly lifts the degeneracy of these two levels. In the autoionizing spectrum, the two levels were very strongly mixed and had nearly equal amplitudes. An interesting aspect of the Sc spectrum is that the oscillator strength was usually much stronger for one of the lines than for the other.

The difference between the experimental and theoretical quantum defects was less than 0.02. These lines were not perturbed by states attached to much higher thresholds which may account for the small errors in the quantum defects. The ^3F target state did not need configuration interaction [1] to achieve the same level of accuracy as the other target states. This suggests that the ^3F target state was more accurate than the $(4s3d)^1D$ or the $(4s^2)^1S$ target states that needed a substantial amount of configuration interaction; we do not expect our model potential for the 18 inner core electrons to be accurate enough to exactly produce the correct configuration for heavily mixed states.

We were unable to classify the $n = 15$ state because it fell too close to three lines of Table 6. The line at 176.217 nm could be the sum of two lines. The $^3F_413p7^o/2$ state is unperturbed and at the correct energy. The $^3F_413p5^o/2$ state is perturbed by the $(3d^2)^1D4f^2D^o$ state and we are therefore not as confident that it is at the correct energy; however, we do not expect the two states to interact very strongly, therefore the two states would need to be nearly degenerate to have a large interaction. This is why we feel the line is probably the sum of the $7^o/2$ and $5^o/2$ lines.

F. Tables 6 and 7 of Garton *et al.*

Table 6 of Garton *et al.* presents lines for which they were only able to classify J_g. The resonances of this table are on Figs. 3 and 4; we marked the experimental positions of (the experimentally classified) $J_g = 3/2$ lines with dash-dot-dot-dot vertical lines and the $J_g = 5/2$ lines with long-dashed vertical lines. We remain unable to classify 8 of these lines. We disagree with the experimental classification for only three of the lines (both columns of the second row and the last row of the second column, i.e., $\lambda = 177.803$ nm, 178.338 nm, and 174.117 nm). The difference between experimental and theoretical quantum defects (calculated as $\Delta\mu = [\Delta\omega\ (\text{a.u.})]\nu^3$) is less than 0.02 for all of the lines and for most of the lines $\Delta\mu \sim 0.01$.

Table 7 of Garton *et al.* presents unclassified lines. The resonances of this table appear on Figs. 3 and 4; we marked the experimental positions of these lines with dotted vertical lines. We can classify all but four of the lines. The errors in the quantum defects are less than 0.02. Several of the lines of this table near 178 nm were characterized as wide or very wide. At this energy is the $(3d^2)^1G5p^2F^o$ perturber which is *extremely* wide ($\sim$ 20 Å) on the scale of the experiment; see Fig. 4. The interaction of the $^3Fnp^2F^o$ states with this perturber gives them a wide or very wide profile.

The two lines at 178.2 and 178.06 nm are very strongly mixed with this perturber; although the autoionizing resonances are at the correct positions they are so broad and heavily mixed with the perturber that the classifications are somewhat meaningless and should only be taken as an indication of which states are being perturbed. The classification for the line at 174.8774 nm is uncertain because of the experimental characterization of the line as being "quite sharp" and having very little oscillator strength. The theoretical classification is for theoretical lines at the correct energy; however, they do not have the experimental character of the observed line. This line is very close to the $(4s^2)4f$ state and it is possible that interactions with this perturber affect the decay rate and oscillator strength of the line; this can account for the theoretical discrepancies.

We have classified all of the lines of Tables 6 and 7 as Rydberg states attached to the $^3F_{J_c}$ thresholds. Most of the states have Rydberg electrons with p-wave character (several have f-wave character). The discussion of the

theoretical accuracy for the lines of Table 5 of Garton *et al.* also applies to the lines of Tables 6 and 7. In fact nearly half of the lines that we could not classify are very close to the $(3d^2)^1D4f^2D^o$ perturbing state.

It is not surprising that the lines of Tables 6 and 7 were not classified by [2]. These are states attached to the spin-orbit split $^3F_{J_c}$ thresholds. The Rydberg series attached to these thresholds interact with each other strongly, producing highly irregular spectra. The purity of the lines is accordingly very low in this region; the classifications give the leading component for each line no matter how low the purity.

G. Unreported lines

There are several prominent theoretical lines of Figs. 1–4 that do not have a corresponding vertical line; the vertical lines indicate the reported positions of experimentally observed resonances. This does not mean that the line was not observed in the experiment. It is clear from Fig. 5 of the previous paper [1] that all of the major features of the theoretical cross section in the range 189.0–185.2 nm are in good agreement (in position and width) with features of one of the experimental plates. For example, there are nine lines below the $(4s3d)^1D$ threshold on plate 2 of Garton *et al.* that are very intense and broad and marked with an F on the plate. Not all of the wavelengths for these lines were reported. We do not feel we can determine the wavelengths of the unreported lines from the plates with sufficient accuracy, therefore we did not mark their positions on the figures. As examples, two of these lines are at $\sim$ 187.9 nm and $\sim$ 185.2 nm. These correspond to two intense and broad features of the theoretical cross section near 187.8 [$3/2 \rightarrow 3^o/2$ $(4s3d)^1D9p^2D$] and 185.2 nm [$3/2 \rightarrow 3^o/2$ and $5/2 \rightarrow 5^o/2$, both the $3^o/2$ and $5^o/2$ final states are strong mixtures of $(4s3d)^1D9p^2D$ and $(3d^2)^3F7p^2D$]. As another example, the theoretical cross sections and the plate show three sharp lines near 185.4 nm, whereas the positions of only two of the sharp lines were reported.

V. SUMMARY

We have presented the theoretical ground state photoionization spectrum in the energy range from the ^3D to the ^3F thresholds, and marked the positions of many autoionizing levels observed by Garton *et al.* [2] for comparison. From the comparison of theoretical and experimental lines far from perturbers, it appears that the errors in the theoretical, short-ranged scattering parameters are less than $\sim$ 0.03. Near perturbers the errors in quantum defects can be larger due to the relatively large errors in the positions of perturbers that are magnified by their large binding energies.

This work has classified most of the autoionizing lines observed by Garton *et al.* [2]. The number of lines that we were able to classify depended on the accuracy of the short-ranged scattering parameters; the comparatively high level of accuracy achieved for the scattering parameters was crucial for the classification. We would (probably) not have been able to classify most of the lines if the calculated quantum defects had errors greater than $\sim$ 0.06. It may be that the added information on the shapes and widths of resonances obtained from numerical cross section data will relax some of the requirements on the level of accuracy needed for the calculated scattering parameters. However, it should be remembered that the shapes of autoionizing states depend on interferences between different channels and therefore the individual resonances may appear quite differently if the perturbers are not at the correct energy. The spectra of most other transition metals will be even more complicated than those presented here; it is only reasonable to assume that for a sensible theoretical description of these atoms the calculations will need to maintain the level of accuracy achieved for Sc. This goal will be more difficult to reach for open-shell atoms with more d electrons.

ACKNOWLEDGMENTS

This research is supported by the Division of Chemical Sciences, Office of Basic Energy Sciences, Office of Energy Research, U.S. Department of Energy Grant No. DE-FG-02-90ER14145.

* Present address: Department of Physics, Auburn University, Auburn, AL 36849-5311.

[1] F. Robicheaux and C.H. Greene, preceding paper, Phys. Rev. A **48**, 4429 (1993).
[2] W.R.S. Garton, E.M. Reeves, F.S. Tomkins, and B. Ercoli, Proc. R. Soc. London, Ser. A **333**, 1 (1973).
[3] F. Robicheaux and C.H. Greene, Phys. Rev. A **46**, 3821 (1992); *ibid.* **47**, 1066 (1993).
[4] F. Robicheaux and C.H. Greene, Phys. Rev. A **47**, 4908 (1993).
[5] C.H. Greene and M. Aymar, Phys. Rev. A **44**, 1773 (1991), and references therein.
[6] C.H. Greene and L. Kim, Phys. Rev. A **38**, 5953 (1988).
[7] U. Fano and A.R.P. Rau, *Atomic Collisions and Spectra* (Academic, Orlando, 1986); M.J. Seaton, Rep. Prog. Phys. **46**, 167 (1983).
[8] A.R.P. Rau and U. Fano, Phys. Rev. A **4**, 1751 (1971); C.M. Lee and K.T. Lu, *ibid.* **8**, 1241 (1973).
[9] J. Sugar and C. Corliss, J. Phys. Chem. Ref. Data, **14**, Suppl. No. 2 (1985).
[10] D. Armstrong and F. Robicheaux, following paper, Phys. Rev. A **48**, 4450 (1993).